On Site-Selective Optically and Thermally Induced Processes in Lu_2O_3:Tb,Ta Storage Phosphors

Paulina Bolek, Dagmara Kulesza and Eugeniusz Zych*

Faculty of Chemistry, University of Wroclaw, 14. F. Joliot-Curie Street, 50-383 Wroclaw, Poland

**eugeniusz.zych@chem.uni.wroc.pl*

Keywords: storage phosphor, carriers trapping, optical bleaching, luminescence

Abstract

Photo- thermo- and optically stimulated luminescence properties of Lu_2O_3:Tb,Ta ceramics sintered at 1700 °C in air were investigated. Low temperature (10 K) excitation and emission spectra using synchrotron excitation in the range of 150-330 nm are also discussed. The effect of the dopant contents on the various luminescence effects and processes was tackled. The ceramics showed intense thermoluminescence (TL) and the glow curve consisted of two main peaks around 170 and 250 °C upon 5 °C/s heating rate. The shape of the glow curve and TL intensity depended strongly on the dopant concentrations. Above 0.1 % of their contents the TL quickly lessened to disappear around 1 %. This was in contrary to photoluminescence which hardly showed any quenching up to the concentration of 1 %. In addition to the regular first order TL kinetics some contribution from tunneling and semi-localized transitions was proved.

1. Introduction

Luminescent materials based on Lu_2O_3 host were reported efficient X-ray phosphors/scintillators, up-converters and storage or persistent luminescence phosphors [1-13]. Trojan-Piegza et al. presented that (Tb^{3+},M^{2+}) co-doped Lu_2O_3 (M=Ca, Sr, Ba) showed efficient persistent luminescence with intense thermoluminescence (TL) around 100 °C [11][12][14]. When the co-dopant was changed into Hf(IV) the persistent emission practically disappeared in favor of a permanent energy storage in deeper traps clearly connected with the Hf(IV) impurity [4][13][15][16]. These observations proved that aliovalent impurities generated point

defects at which excited charge carriers could be efficiently trapped. Tb^{3+} ions produced the thermoluminescence photons and – in agreement with the Dorenbos model [17–23] – served as hole-trapping centers. The co-dopants were thus linked – directly or indirectly - with electron-trapping sites.

Recently, scant TL characteristics of Lu_2O_3:Tb,Ta ceramics have been presented [24]. The glow curves, fading and kinetics order of persistent luminescence were there discussed. Hole trapping at $Tb_{Lu}^{\times}$ and electron trapping at $Ta_{Lu}^{\cdot\cdot}$ were there postulated and the latter was supposed to immobilize one or two electrons being converted into $Ta_{Lu}^{\cdot}$ or $Ta_{Lu}^{\times}$, respectively. It is important to characterize and understand TL of these ceramics in depth. Together with data on other storage phosphors utilizing Lu_2O_3 host this should make it possible to define what all of them have in common in terms of physics standing behind their TL-related properties. As indicated in [25–28] TL materials with TL at quite different temperatures (like the 170 °C and 250 °C in our case) might be useful to sense thermal history in harsh conditions. This makes the Lu_2O_3:Tb,Ta ceramics interesting also from the practical point of view.

In this paper we concentrate mainly on tracking the carriers pathways when released by means of thermal or optical stimulation. Attention will also be given to profound effect of dopant contents to the storage properties, which is in contrast with photoluminescence dependence on this parameter. Systematic analysis of effects of heating rate, fading and persistent luminescence decay kinetics and controlled optical bleaching for different concentrations of Tb and Ta dopants are also discussed.

2. Experimental Section

Lu_2O_3:Tb,Ta sintered ceramics were prepared using powders made by Pechini method [29]. The concentrations of Tb and Ta were in the range of 0.025-1 mol% with respect to Lu. The procedure was analogous to described in [24]. Shortly, lutetium(III) nitrate pentahydrate ($Lu(NO_3)_3*5H_2O$ (99.99%)), terbium(III) nitrate hexahydrate ($Tb(NO_3)_3*6H_2O$ (99.99%)) and tantalum(V) chloride ($TaCl_5$ (99.95%)) were were diluted in 2 M solution of citric acid. Next, some ethylene glycol was added. Upon slow condensation and final heating at 700 °C raw powders were obtained. 0.25-0.30 g portions of obtained powders were pressed into pellets 8 mm in diameter under the load of 4 tons for 5 minutes. These pellets were sintered in corundum crucibles at 1700 ^oC for 5 hours in air. The heating and cooling rates were 3 ^oC/min.

Crystallographic purity of all ceramics was checked by means of powder X-ray diffraction (XRD) technique in the range of 2θ=10-80^o using D8 Advance diffractometer from Bruker. Photoluminescence spectroscopic experiments were performed using FLS980 spectrofluorometer from Edinburgh Instruments Ltd. Excitation spectra were corrected for the incident light intensity and emission spectra for the emission channel spectral efficiency. Some PLE spectra were taken at 200 K. The sample was then cooled using closed-cycle helium cryostat from Lake Shore Cryotronics LTd. Thermoluminescence glow curves were measured in the rage of 30-500 ^oC after irradiation of the ceramics with 254 nm radiation from mercury lamp. The custom made thermoluminescence set up consisted of a temperature controller with linear heating rate and Ocean Optics HR2000 CG spectrometer operating under the control of OOIBase dedicated software. The thermoluminescent photons were collected with a 74-UV lens coupled to a QP600-1-SR waveguide which transferred the light to the spectrometer equipped with a CCD camera operating in the range of 200-1100 nm. The TL spectra and the data for glow curves were collected every 1 s during the TL measurement. Heating rate was typically 4.7 ^oC/s. To register effect of heating rate on TL, three heating rates were used 1, 4.7

and 8.9 °C/s. Optical bleaching was measured after exposure of the sample to 254 nm radiation for 10 seconds followed by prolonged stimulation (bleaching) with either 980, 780 or 430 nm laser diodes light. Optically stimulated luminescence (OSL) decay traces and spectra were registered for X-ray irradiated specimens upon stimulation with 980, 780 or 430 nm radiation from laser diodes. The OSL decays were taken monitoring luminescence at 542.4 nm ($Tb(C_2)$ site) and 544.0 nm ($Tb(C_{3i})$ site). The OSL signal was collected with the same OceanOptics CCD camera which collected data every 1 s.

The emission and luminescence excitation spectra were measured using synchrotron radiation in DESY at the SUPERLUMI station in the HASYLAB laboratory in Hamburg [30]. Measurements were performed at 10 K with variable step in the range of 0.1 to 1.0 nm and with counting time of 0.5 s. The spectra were corrected for the variations in the incident light intensity using sodium salicylate as a standard. Emission spectra upon the synchrotron radiation excitation were measured with a high-resolution (~0.05 nm) CCD camera using a grating with 1200 grooves/mm.

3. Results

For all samples the phase purity was checked by powder XRD technique and no indication of foreign phase(s) was observed as already discussed in [24]. All specimens crystallized in the cubic C-type structure [31][32]. This indicates that both the $Ta_{Lu}^{\bullet\bullet}$ defect and the necessity to compensate its extra charge by yet another defect(s), presumably interstitial oxygen ($O_i^{''}$), could be effectively accommodated by the lutetia host. The two metal sites present in Lu_2O_3 [31][32], C_2 and C_{3i}, are located in centre of cubes whose only six corners are filled with oxygen atoms while the other two are empty [31][32]. Therefore, compensation of the additional charge of the $Ta_{Lu}^{\bullet\bullet}$ point defect by $O_i^{''}$ is most feasible.

3.1. Photoluminescence

In contrast to Lu_2O_3:Eu [33–35], the scientific literature lacks presentation of comprehensive site-selective spectroscopic data of Lu_2O_3:Tb. However, for understanding of the various TL and OSL results it is essential to recognize photoluminescence properties of the Lu_2O_3:Tb,Ta ceramics. First we shall present excitation and high resolution emission spectra taken at 10 K using synchrotron radiation for excitation in Fig. 1a,b.

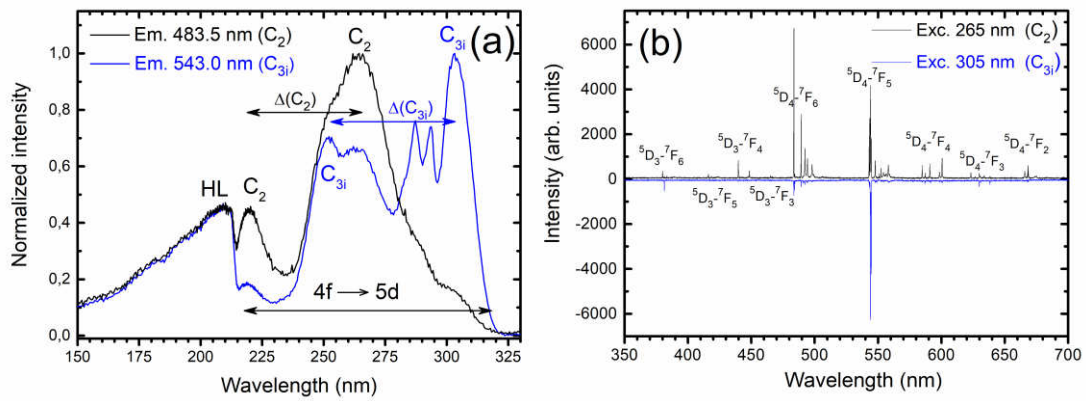

Fig. 1. (a) 10 K excitation spectra of the 483.5 nm ($Tb(C_2)$) and 543.0 nm ($Tb(C_{3i})$) luminescence. (b) high resolution emission spectra registered upon 265 nm ($Tb(C_2)$) and 305 nm excitation ($Tb(C_{3i})$).

Fig. 1a depicts 10 K excitation spectra of the 483.5 nm (mainly $Tb(C_2)$) or 543 nm (mainly $Tb(C_{3i})$) emissions in the range of 150-330 nm wavelengths. The assignment was inferred from emissions presented in Fig. 1b. It is important to realize that truly site-selective observation of the centrosymmetric $Tb(C_{3i})$ was not possible, but reasonable selectivity was reached. Consequently, 4f→5d excitation bands observed in the 215-325 nm range of wavelengths could be reliably assigned to either $Tb(C_2)$ or $Tb(C_{3i})$, see Fig. 1a. In the case of the former the splitting of the 5d levels in crystal field ranges at 10 K from ~220 nm to ~265 nm which gives $\Delta(C_2)$ = 0.96 eV. Analogously, the most separated components for the $Tb(C_{3i})$ peak at 251 nm and 304 nm which gives $\Delta(C_{3i})$ = 0.86 eV. Both are reasonable values in an oxide host.

These results prove that the lowest $5d_1$ level of the Tb(C_2) is positioned by about 0.6 eV higher than its correspondent level of Tb(C_{3i}). The host lattice absorption starts at 212 nm which agrees with position of free exciton absorption in Lu_2O_3 [36]. Assuming after Dorenbos that the average bounding energy of free exciton in insulators is about 8 % of the host band gap energy (E_g) the latter can be estimated at 6.2-6.3 eV. All these data were transferred to a scheme of Vacuum Referred Binding Energies (VRBE) developed by Dorenbos [20][37], see Fig. 2. It presents for the first time vacuum referred electronic levels of the Lu_2O_3:Tb system taking into account the differences between the Tb(C_2) or Tb(C_{3i}) sites.

High resolution emission spectra (Fig. 1b) confirm that Tb^{3+} occupies both symmetry sites offered by the host lattice. Emission of the centrosymmetric Tb(C_{3i}) at 10 K is mostly located around 545 nm where the $^5D_4 \rightarrow {}^7F_5$ magnetic dipol ($\Delta J=1$) transition appears. In contrary, the 10 K luminescence of the Tb(C_2) is much richer and its most profound lines result from the $^5D_4 \rightarrow {}^7F_6$ hyper-sensitive ($\Delta J=2$) transition. Assignment of the emission lines is given in Fig. 1b.

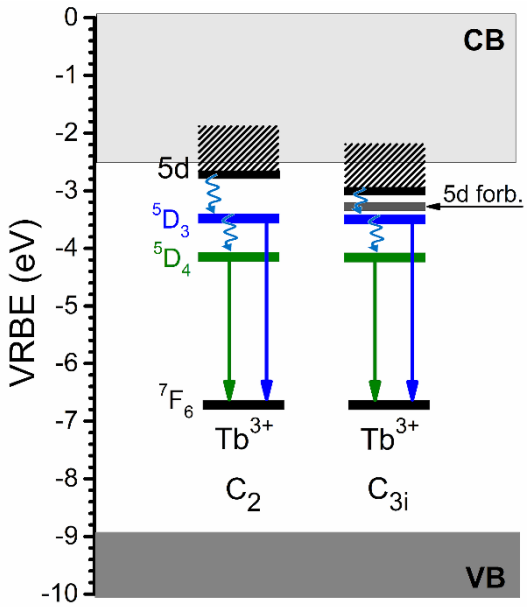

Fig 2. VRBE level schemes of Lu_2O_3:Tb ceramic phosphor showing – derived from experiments with synchrotron radiation - differences between position of 5d levels of the Tb(C_2) and Tb(C_{3i}) ions.

Fig. 3a shows room temperature excitation spectra of emissions monitored at wavelengths of the most characteristic luminescence features of the two Tb^{3+} sites, C_2 and C_{3i}, shown in Fig. 3b. Additionally (broken lines), in Fig. 3a excitation spectra of Lu_2O_3:Tb,Ta previously irradiated at 270 nm (preferentially Tb(C_2)) or 310 nm (Tb(C_{3i})) are shown. Since after such irradiation the sample showed significant afterglow at room temperature (RT) it was cooled to 200 K before taking these two excitation spectra. Note that position of the various features at room temperatures are slightly different than at 10 K (Fig. 1a,b).

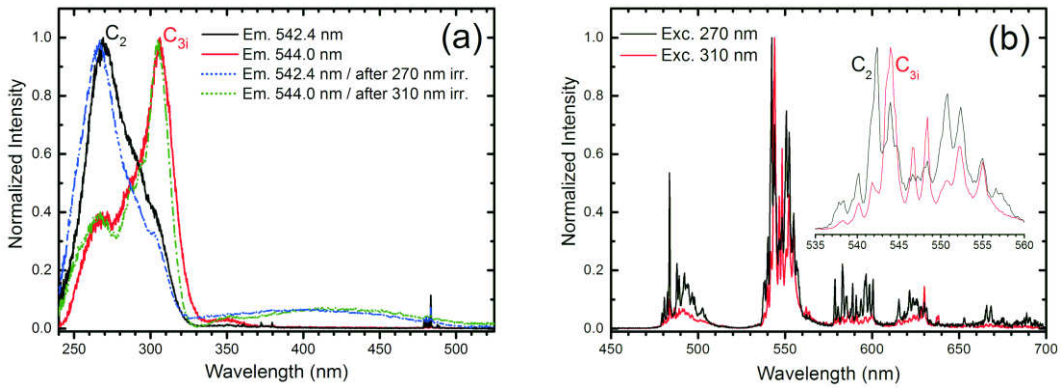

Fig. 3. *(a) RT Excitation spectra of the 542.4 and 544.0 nm luminescence for Lu_2O_3:Tb,Ta raw specimen and recorded at 200 K after exposure at RT to 270 and 310 nm irradiation (dotted lines). (b) Emission spectra registered upon 270 nm (Tb^{3+} in C_2 site) and 310 nm excitation (Tb^{3+} in C_{3i} site). Excitation at 350 nm produces emission (not shown) very similar to that excited at 310 nm.*

Both excitation spectra of non-irradiated sample consist of a broad band in the ~270-340 nm range of wavelengths which comes from the spin-allowed $4f^8 \rightarrow 4f^7 5d^1$ transition. The maximum is either around 270 nm or at 305 nm for 542.4 nm and 544.0 nm emissions, respectively. The former is characteristic for the Tb(C_2) and the latter for the Tb(C_{3i}). This assignment will be further justified upon the differences of the two emissions kinetics, as presented in Fig. 4a,b. Electric dipole induced emission transition of the Tb(C_2) decays much faster than luminescence of Tb(C_{3i}) which is mainly magnetic dipole transition in character [38]. A low-intensity excitation band peaking at 350 nm in the case of the Tb(C_{3i}) excitation spectrum results from the spin-forbidden $4f^8 \rightarrow 4f^7 5d^1$ transition firstly observed and discussed for the second half of

lanthanides by Meijerink [39][40]. Excitation into this feature produces emission from $Tb(C_{3i})$, exclusively (not shown). Note that analogous transition for the $Tb(C_2)$ has to occur around 310 nm where it overlaps with the allowed intense 4f→5d excitation of $Tb(C_{3i})$. At yet longer wavelengths 4f→4f narrow lines of very low intensities are observed in all excitation spectra. Their detailed analysis reveals differences in the position of the 4f→4f excitation features for the two Tb^{3+} sites. As expected [38], the relative intensity of the 4f→4f lines to the 4f→5d bands is clearly higher in $Tb(C_2)$ compared to $Tb(C_{3i})$. This occurs as the 4f→4f excitation/absorption transition rates for the centrosymmetric $Tb(C_{3i})$ site are much lesser than for the $Tb(C_2)$ [38].

Interesting changes in excitation spectra are observed after exposure of the sample to 270 nm or 310 nm radiation for a few minutes prior to the measurement, see the broken lines in Fig. 3a. Namely, these spectra contain a new extremely broad band of moderate intensity extending from quite deep UV up to above 500 nm at least. This band indicates that a new excitation pathway of Tb^{3+} emission is activated in the irradiated sample and that it is directly connected with changes which were induced in the material by means of the short-wavelengths UV photons used for its irradiation. As will be shortly seen, this excitation feature has to be connected with releasing of electrons formerly (during irradiation) trapped at the $Ta^{\bullet\bullet}_{Lu}$ co-dopant sites. In the course of stimulation into this band the Tb^{3+} emission continuously weakens and finally disappears as well as the induced excitation band. Unfortunately, our system does not allow to record reliable excitation spectra at wavelengths longer than the emission of Tb^{3+} (>~600 nm) in deep red and infrared part of spectrum. Nevertheless, later we will show that some excitation features induced by irradiation with the UV photons (or X-rays) have to be present there too.

In Fig. 3b emission spectra of Lu_2O_3:Tb,Ta upon excitation of the $Tb^{3+}(C_2)$ (270 nm) and $Tb^{3+}(C_{3i})$ (310 nm) are presented. Both spectra consist of sharp lines in the range of 470-700 nm resulting from the $^5D_4 \rightarrow {}^7F_J$ transitions of Tb^{3+} ions. The most intense emission features of $Tb(C_2)$ and $Tb(C_{3i})$ are located around 550 nm resulting from the $^5D_4 \rightarrow {}^7F_5$ transition. Lines of both Tb^{3+} sites are thoroughly mixed and not well separated. Yet, two of them were found useful to track semi-selectively emissions from the two sites. They are located at 542.4 nm and 544.0 nm for $Tb(C_2)$ and $Tb(C_{3i})$, respectively (see Fig. 3b). They were used to record the relavent excitation spectra (Fig. 3a) already discussed above.

Decay traces of emissions from both sites were measured for concentrations spanning the range of 0.05-1 mol%. In the case of the $Tb(C_2)$ luminescence (Fig. 4a) no concentration quenching is observed. The $Tb(C_{3i})$ emission (Fig. 4b) shows some concentration quenching but it does not exceed ~15 % comparing the 1 % sample to the 0.05 % one. Up to 0.5 % the effect is marginal at most. Decay traces were also measured at higher temperatures, up to 500 °C and they showed thermal quenching very similar to reported in [4] based on the PL intensity temperature dependence. Finally, the Tb^{3+} emission practically disappears above 400 °C.

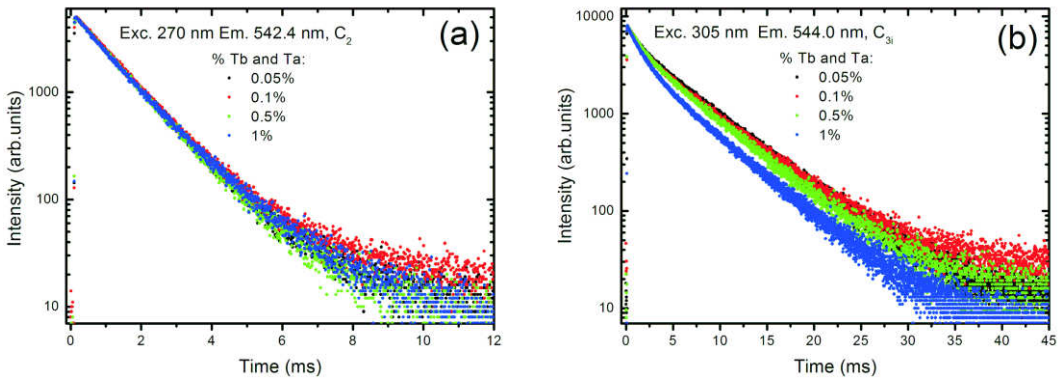

Fig. 4. *(a) Luminescence decay curves of Lu_2O_3:Tb,Ta with different content of the dopants (given in the figure). (a) excited at 270 nm and monitoring the luminescence at 542.4 nm for $Tb(C_2)$ and (b) excited at 305 nm and recording the emission at 544.0 nm for $Tb(C_{3i})$*

Tab. 1. *Average decay times of photoluminescence of Lu_2O_3:Tb,Ta ceramics.*

Composition	Average decay time (ms)	
	Exc. 270 nm Em. 542.4 nm (C_2)	Exc. 305 nm Em. 544.0 nm (C_{3i})
0.05% Tb, 0.05% Ta	1.40	5.40
0.1% Tb, 0.1% Ta	1.45	5.30
0.5% Tb, 0.5% Ta	1.30	5.00
1% Tb, 1% Ta	1.35	4.45

3.2. Thermoluminescence

Fig. 5a,b presents TL glow curves of Lu_2O_3:Tb,Ta ceramics with different concentrations of the activators. In Fig. 5a the Tb content is 0.05 % and Ta concentration spans the range of 0.025-1.0 % and in Fig. 5b the Ta concentration is 0.05 % and percentage of Tb spreads over the range of 0.025-0.2 %. These curves are much different from the TL glow curve of singly doped Lu_2O_3:Tb ceramics presented previously [24]. This proves that Ta addition indeed affects the storage properties in Lu_2O_3:Tb,Ta. Importantly, whatever the concentrations are the TL glow curves present exactly the same shape with two TL components representing two traps of different depths. They peak at ~170 °C and ~250 °C. All these observations tell to conclude that this is Ta which shapes the trap depths in Lu_2O_3:Tb,Ta ceramics. In contrary, it is easy to note that the *efficiency* of energy storage *is* strongly dependent on the dopant contents being the highest when both activators are present in small concentrations of about 0.05 %.

In Fig. 5c the effect of dopant concentrations on the TL of the Lu_2O_3:Tb,Ta ceramics is further studied – now both dopants have the same contents between 0.05 % and 1.0 %. It is immediately seen that the TL intensity drops quickly as the dopant contents increase and for 1 % sample TL practically disappears. TL of the 0.5 % sample is by a factor of ~5 lower than TL of the 0.05 % ceramics. This accords with results presented in Fig. 5a,b and upon the photoluminescence data presented above (see Fig. 4) this effect cannot be connected with a concentration quenching of the Tb^{3+} luminescence. Then, we have to conclude instead that a concentration-induced

extinguishing of carriers trapping in their relevant traps occurs. This is a clear sign that for efficient carriers trapping/energy storage the dopant trapping sites have to be distanced enough to make their interaction negligible. Another possibility is that with increasing concentration of the dopants they tend to aggregate or cluster reducing the permanent carriers trapping capability.

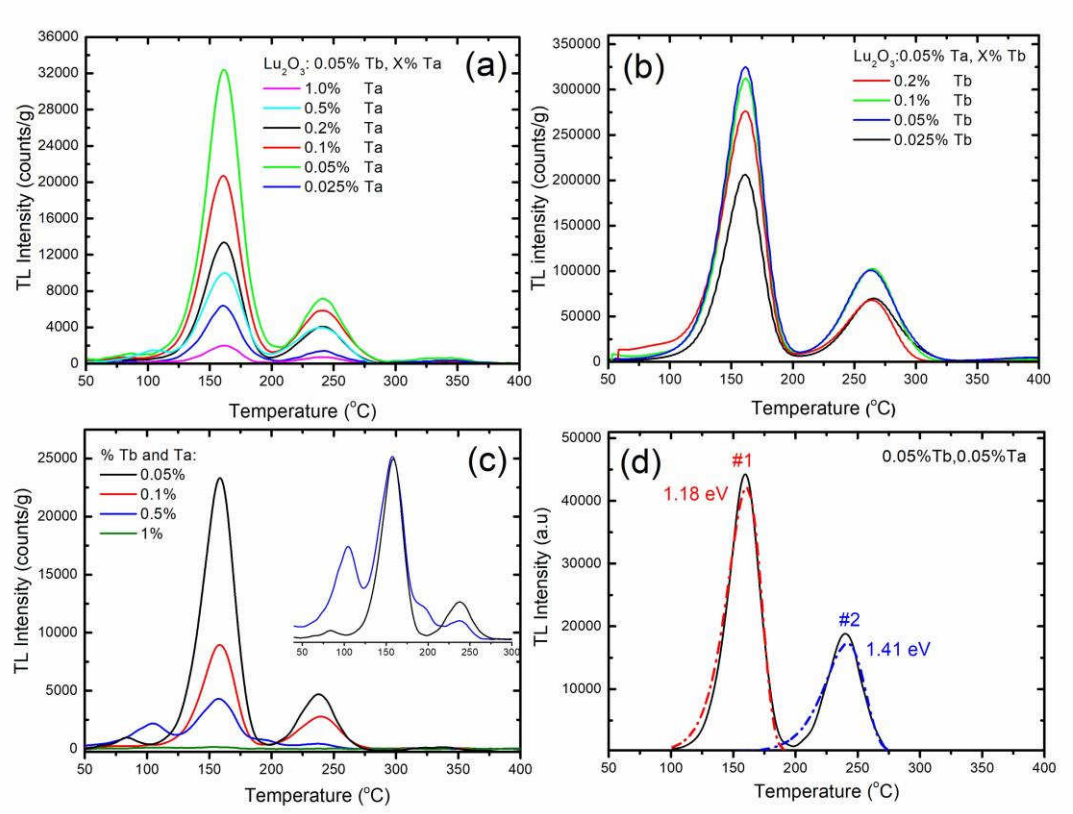

Fig. 5. *(a-c) Concentration dependence of TL glow curves of Lu_2O_3:Tb,Ta ceramics (not corrected for thermal quenching of Tb^{3+} PL) registered after 254 nm irradiation. The inset in (c) shows normalized TL glow curves of the 0.05 % and 0.5 % samples. (d) Deconvolution of TL glow curve of Lu_2O_3:0.05%Tb,0.05%Ta ceramics – see text for details. TL glow curve was corrected for thermal quenching of Tb^{3+} PL.*

Not only is the glow curve of the 0.5 % ceramics much less intense than the 0.05 % but also its shape is more complex compared to the diluted system. A relatively significant component around 100 °C and a shoulder around 190 °C are present only in the TL glow curve of the 0.5 % ceramics. All that points that the reduced distance between dopants (=traps) generates

interactions which diminishes the capability of carriers trapping in the system. Taking into account data presented in Fig. 5a,b this effect has to be assigned to interaction between Tb^{3+} ions at first, as higher content of Ta does not cause similar effects.

It was shown in our previous paper [24] that the TL of Lu_2O_3:Tb,Ta is governed by the first order kinetics and the main TL peaks result from continuous distribution of traps having similar but not identical energies. Consequently, the shape of the peaks differ significantly from the profile predicted by the *One Trap One Recombination* center (OTOR) model of the first order kinetics developed by Randall and Wilkins [41][42]. This is well expressed by the geometry factor, μ_g, [43] defined by Eq. 1:

$$\mu_g = \frac{\delta}{\omega}, \tag{1}$$

where δ stands for the half maximum width of the high-temperature fraction of the TL peak and ω represents its full width at half maximum. Ideally, a single trap of the first order kinetics gives $\mu_g = 0.42$ [43]. The Ta-related most intense peaks in Lu_2O_3:Tb,Ta have $\mu_g = 0.48$ (~170 °C) and $\mu_g = 0.52$ (~250 °C). These much higher values are understandable from the distribution of trap energies as just mentioned. Yet, some contribution to the shape of the measured TL peaks results from occurrence of semi-localized transitions, which will be proved and discussed shortly.

From the above conclusions, fitting the TL peaks using the first order kinetics approach cannot bring precise values of the trap depths. Yet, just to get general indications of their parameters the glow curve of the diluted sample (after correction for thermal quenching of PL) was fitted using arbitrary two components and frequency factors fixed at 1.7×10^{13} s^{-1} reflecting the 580 cm^{-1} fundamental vibrations of the Lu_2O_3 host [44]. The result is presented in Fig. 5d. Such an appraisal gives trap depths of 1.18 eV and 1.41 eV for the $Ta_{Lu}^{\bullet\bullet}$ and $Ta_{Lu}^{\bullet}$ traps showing TL at 170 °C and 250 °C, respectively. It is noteworthy that both simulated peaks in Fig. 5d are

broader than the measured ones even though the latter represent some distribution of traps [24]. This clearly indicates that the effective frequency factor, *s*, is higher than just calculated from the host vibrations. This further infers that the TL process is more complex than assumed in the pure first order kinetics.

To further trace the TL-related processes in Lu_2O_3:Tb,Ta the dependence of their TL on heating rate, β = 1, 4.7 or 8.9 °C/s, was measured for the 0.05 % (Fig. 6a) and 0.5 % (Fig. 6b) ceramics. The recorded TL glow curves were corrected for the thermal quenching of the photoluminescence of Tb^{3+} ions to account for the loss of emitted light due to this quenching pathway. According to Randall-Wilkins model of first-order TL kinetics the (integrated) intensity of TL glow peaks should be independent on heating rate and only the TL maxima should shift towards higher temperatures with increasing rates [42][45–47]. Clearly, Lu_2O_3:Tb,Ta storage phosphors do not satisfy all these conditions.

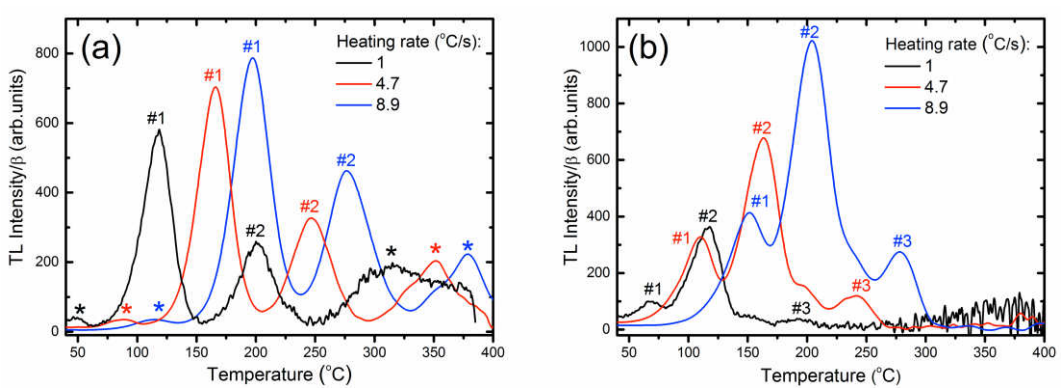

Fig. 6. *TL glow curves of (a) Lu_2O_3:0.05%Tb,0.05%Ta (b) Lu_2O_3:0.5%Tb,0.5%Ta registered with different heating rates. TL glow curves were corrected for thermal quenching of PL Tb^{3+}.*

As seen in Fig. 6, with increasing heating rate a noticeable growth of intensities of the two main TL bands, #1 and #2, was clearly discerned in both compositions – 0.05 % and 0.5 %. For the 0.5 % sample all three peaks, #1 , #2 and #3, showed such behavior. In contrary, the low-intensity, low-temperature TL component in Fig. 6a (denoted with *) as well as the high-temperature peak above 300 °C (also marked with *) behave differently. Their intensities,

within the experimental error, are not dependent on the heating rate. This is consistent with the previous assignment of only peaks #1 and #2 (and #1, #2 and #3 for the 0.5 %) to Ta co-doping in these ceramics. They clearly share some important characteristics.

The effect of increase of TL glow peak intensity with increasing heating rate is known as anomalous heating rate dependence. It is quite a rare case in TL materials [48–52]. When anomalous heating rate occurs it is often connected with anomalously high fading even from deeper traps. The later was explained as a result of leakage of trapped electrons to holes by a localized (and rather nonradiative) mechanism [48–50]. This effect was theoretically and experimentally extensively treated by Mandowski and Bos for YPO_4:Ce,Sm [50]. It was further developed into a consistent theory of semi-localized transitions (SLT) by the former [48–50].

The SLT model assumes occurrence of two pathways of recombination of trapped carriers upon heating: (i) a regular delocalized route when electron is raised to the conduction band to further diffuse to the luminescence center (the hole trap) and (ii) competitive localized (so distance-dependent) process with a low energy barrier of direct electron-hole recombination of nonradiative character. For low heating rates overall efficiency of the latter is relatively significant compared to the former. When the heating rates are high, relative efficacy of the former increases making the radiative relaxation efficiency higher. This is exactly what is observed in the Lu_2O_3:Tb,Ta ceramics. Noteworthy, between peaks #2 and #3 a shoulder is observed for the more concentrated (0.5 %) system (Fig. 6b). The appearance of such a peak is anticipated by the SLT model [50]. Furthermore, SLT mechanism affects the shape of the TL peak making it more symmetrical than in regular first order kinetics [50]. Nevertheless, purely SLT mechanism still leads to some asymmetry of the TL peak with the higher-temperature part narrower. From the data presented in [50] we estimated the asymmetry parameter μ_g ranging at 0.44-0.47. The even larger μ_g in our Lu_2O_3:Tb,Ta (0.48 and 0.52, see above) has to result from a combined effect of SLT and continuous distribution of trap energies [24].

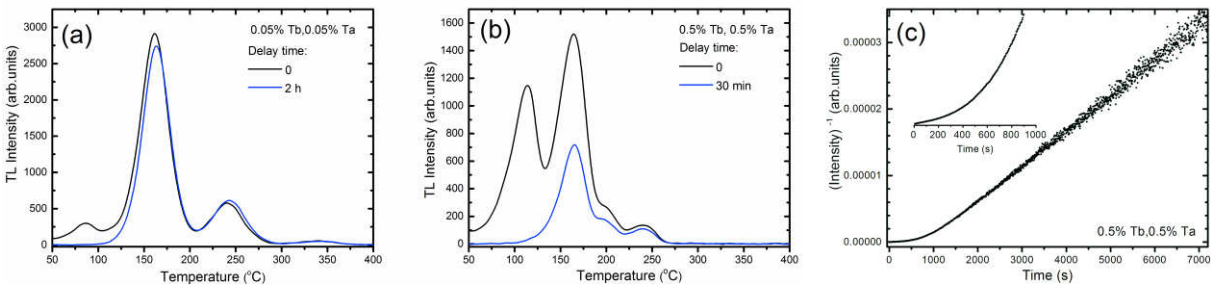

Fig. 7. *Fading of TL for two (a) low and (b) high concentrated compositions of Lu_2O_3:Tb,Ta. Fading was registered at RT after irradiation of the samples with 254 nm radiation. (c) I^{-1}vs.time dependence of the afterglow signal of the 0.5 % sample. Decay of afterglow was measured after 270 nm irradiation of the sample.*

As just mentioned, the presence of SLT mechanism should lead to quickly growing fading of the TL signal with increasing population of the trapping sites – Tb^{3+} and Ta(V) activators [48–50]. In Fig. 7 RT fading of both compositions (0.05% and 0.5%) is presented. For the diluted system (Fig. 7a) fading within the first 2 hours appeared negligible. Low intensity peak around 70-80 °C obviously disappeared, but the main Ta-related peaks around 170 °C and 250 °C practically retained their intensities. Such behavior was expected, as – according to Arrhenius equation the lifetime of the 1.18 eV trap (170 °C) is τ = 1480 hours at RT.

The more concentrated sample showed a very significant fading already during the first 30 minutes after ceasing its irradiation. Not only the low-temperature peak around 100 °C disappeared but also the peak at 170 °C lost almost 50% of its original intensity within such a short time. Only the weaker component (#3 in Fig. 6) around 250 °C was more resistant to fading in the 0.5 % ceramics. The fading from the 0.5 % material is at least partially radiative, as seen in Fig. 7c, which presents the afterglow luminescence intensity dependence on time drawn as a function of $I^{-1}(t)$. The apparently linear relations indicates that the process occurs mainly by tunneling, a strongly distance-dependent mechanism [45]. These results accord with the preliminary conclusion presented above that the separation of electron and hole traps is a key factor affecting the ability of long-term carriers immobilization in Lu_2O_3:Tb,Ta ceramics. Only traps distanced enough to not interact may store carriers for a long time.

3.3 Optically stimulated luminescence

The trapped carriers may be freed from their traps not only thermally but also (though not in all storage phosphors [53]) by means of optical stimulation. Optical bleaching with 980, 780 and 430 nm radiation was conducted for the diluted sample after its irradiation with short-wavelength UV photons.

During prolonged stimulation with 980 nm radiation (~1.26 eV, Fig. 8a) the TL around ~170 °C totally disappeared indicating that such photons carry enough energy to release electrons from this trap. Simultaneously, the TL at 250 °C was also partly reduced although it retained about 30 % of its original intensity even after 6 hours of such stimulation, see Fig. 8b. This indicates that the energy of 1.26 eV radiation hardly meets the optical depth of the deeper trap, presumably $Ta^{\bullet}_{Lu}$, and the carriers escape this trap upon such photons with a very low rate then. These results accords with trap depths, 1.18 eV and 1.41 eV, estimated from fitting the glow curve (Fig. 5b). This explains why only the shallower trap can be effectively emptied with the 980 nm (1.26 eV) radiation.

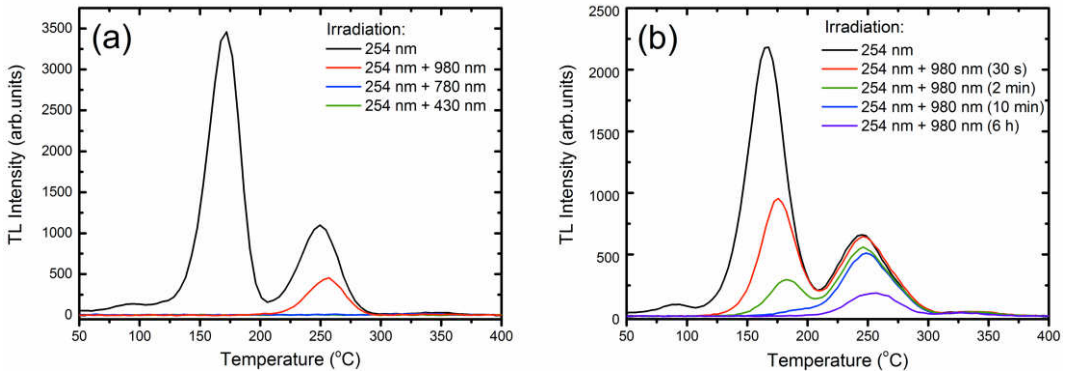

Fig. 8. *Effect of optical bleaching on TL glow curves of 0.05 % ceramics registered after irradiation with 254 nm and subsequent stimulation (bleaching) with (a) 980, 780 or 430 nm light for 30 minutes or with (b) 980 nm light for different periods of time.*

After stimulation with ~780 nm radiation (~1.59 eV) both main TL peaks totally disappeared, see Fig. 8a. Thus, the 1.59 eV photons are capable of releasing trapped carriers from both main traps easily. This accords with the fact that even the deeper trap is shallower (1.41 eV) than the

energy carried by the 780 nm radiation. Efficient bleaching of the traps was also obtained upon 430 nm (2.88 eV) stimulation - into the broad absorption/excitation band induced by short-wavelength UV or X-rays seen in excitation spectra (see Fig. 3a). The very broad range of energies covered by this band (at least ~2.5-3.85 eV; ~500-320 nm, see Fig. 3a) may indicate the excitation of trapped carriers above the bottom of conduction band giving them higher mobility and allowing for their more effective diffusion to the $Tb^{\bullet}_{Lu}$.

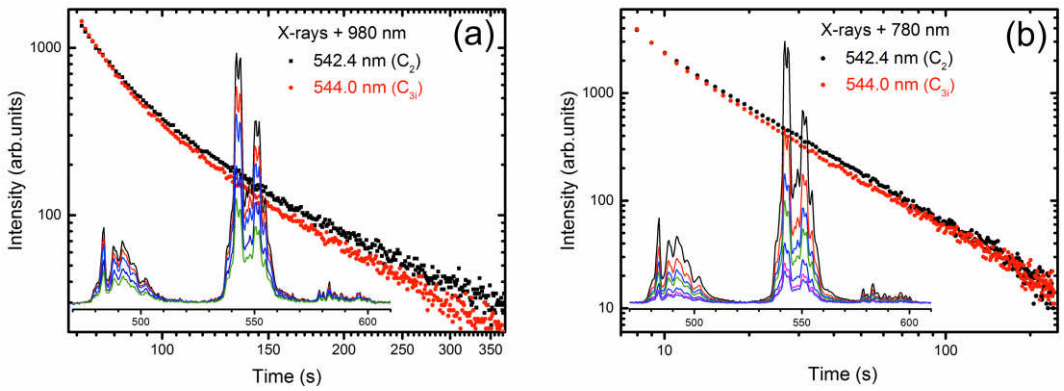

Fig. 9. *Decay curves of 0.05 % ceramics OSL registered after irradiation samples with X rays and prolonged stimulation with (a) 980 nm and (b) 780 nm plotted in double log scale. Inset shows emission spectrum registered during decay measurement.*

Figs. 9 and 10 present more data on the OSL emissions and their kinetics upon 980, 780 and 430 nm stimulation. All traces are strongly non-exponential. Therefore the decay curves of OSL emissions of $Tb(C_2)$ and $Tb(C_{3i})$ upon stimulation with 980 nm radiation (Fig. 9a) and 780 nm (Fig. 9b) are plotted in fully logarithmic scale. The strongly non-exponential course of both decays indicates that the OSLs are governed by more complex mechanism. Emission spectra registered during the stimulations are displayed in insets. Intensities of generated light continuously decrease as these emissions are fed consuming limited resources of previously trapped carriers. Upon both stimulations (980 or 780 nm, Fig. 9) the emission of $Tb(C_{3i})$ seems to decay slightly faster than $Tb(C_2)$. The difference is, however, indeed minor. In both cases the OSL emissions are generated by Tb^{3+} ions exclusively.

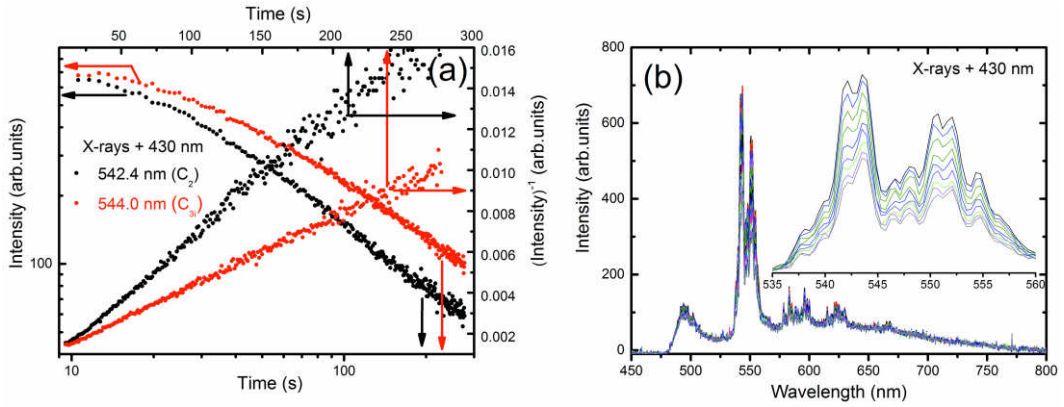

Fig. 10. *(a) Decay curves of 0.05 % ceramics OSL registered after irradiation samples with X rays and prolonged stimulation with 430 nm light plotted in double log scale and inverse of intensity vs time. (b) Emission spectra registered during 430 nm stimulation.*

Analogous OSL experiments were performed using 430 nm stimulation, which was earlier recognized as very efficient in emptying all traps, see Fig. 8a. Such radiation carries much more energy (2.88 eV) than the estimated trap depths. These results are presented in Fig. 10. Upon 430 nm stimulation emission coming from $Tb(C_2)$ (line at 542.4 nm) decays clearly faster than emission of $Tb(C_{3i})$ (line 544.0 nm). This is also well seen in Fig. 10b presenting the spectra generated upon the 430 nm stimulation. The faster decay of the 542.4 nm line upon 430 nm stimulation indicates that $Tb(C_2)$ – precisely, the $Tb^{\bullet}_{Lu}(C_2)$ - is more efficient in capturing of the carriers raised deeper to the conduction band than $Tb^{\bullet}_{Lu}(C_{3i})$.

Consequently, the population of the $Tb^{\bullet}_{Lu}(C_2)$ depletes faster and their relevant contribution to OSL continuously decreases compared to $Tb^{\bullet}_{Lu}(C_{3i})$. Yet, the decay of emission from both sites upon 430 nm drawn as I^{-1} vs. t (Fig. 10a) produced perfectly straight lines within the whole time of the experiment. This is often interpreted as effect of a direct localized electron-hole transition by means of tunneling. In our experimental conditions is unlikely, however. On the other hand, such a dependence can also appear when continuous distribution of traps is present [54] which is our case as reported in [24].

The different kinetics of the emission from the two sites upon 430 nm compared to 980 nm or 780 nm stimulation may be understood assuming that only the former, most energetic, raise the electrons from their traps well above the very bottom of the conduction band (CB). Then, these carriers have possibility to diffuse over larger distances within CB before being captured by $Tb^{\bullet}_{Lu}(C_2)$ or $Tb^{\bullet}_{Lu}(C_{3i})$ compared to carriers released by the much less-energetic photons of 980 nm or 780 nm radiation. Since the lowest excited 5d levels of both $Tb(C_2)$ and $Tb(C_{3i})$ are located just below the conduction band [52] they may be considered thermally coupled with the CB around 300 K. This effectively broadens CB from its bottom side. Consequently, it is possible that carriers excited with 980 nm or 780 nm radiation, maybe a fraction of them, reach *directly* the 5d excited levels of $Tb(C_2)$ and $Tb(C_{3i})$. Altogether, electrons freed upon the 980 nm or 780 nm are expected to migrate over much shorter distances than those liberated upon 430 nm radiation and are supposed to reach $Tb^{\bullet}_{Lu}$ located close/the closest to the electron trap.

4. Discussion

The collected data prove that the main TL peaks located at 170 °C and 250 °C in diluted system (0.05 %) and at 100 °C, 170 °C and 250 °C in the more concentrated one (0.5 %) are due to the Ta co-doping. The 100 °C trap in the former ceramics may come from the Ta-Ta interaction due to their pairing leading to some lowering of the Ta-trap depth. It may also reflect appearance of tantalum-interstitial oxygen ($Ta_{Lu}^{\bullet\bullet}$-$O_i^{''}$) pairs, plausible entities for more concentrated materials. Then, the extra oxygen, $O_i^{''}$, would modify the $Ta_{Lu}^{\bullet\bullet}$ trap properties, as actually observed. Nevertheless, efficient long-term energy storage requires low concentration of the activators. In the more concentrated compositions the carriers leak at RT even from deeper traps and when the dopant contents reach 1 % hardly any energy storage can occur. Consequently, it appears that proximity of the dopants/traps allowing them to interact, makes the permanent trapping continuously less efficient. Presumably, the carriers annihilate without any longer immobilization on traps when they are close each other. This is confirmed by tunneling mechanism of the afterglow connected with the significant fading of the 0.5 % ceramics (see Fig. 7c). Contribution of the SLT mechanism also accords with the low efficiency of carriers trapping in the more concentrated systems. All that processes are schematically presented in Fig. 11. For clarity, this figure does not differentiate between the two Tb sites (see Fig. 2).

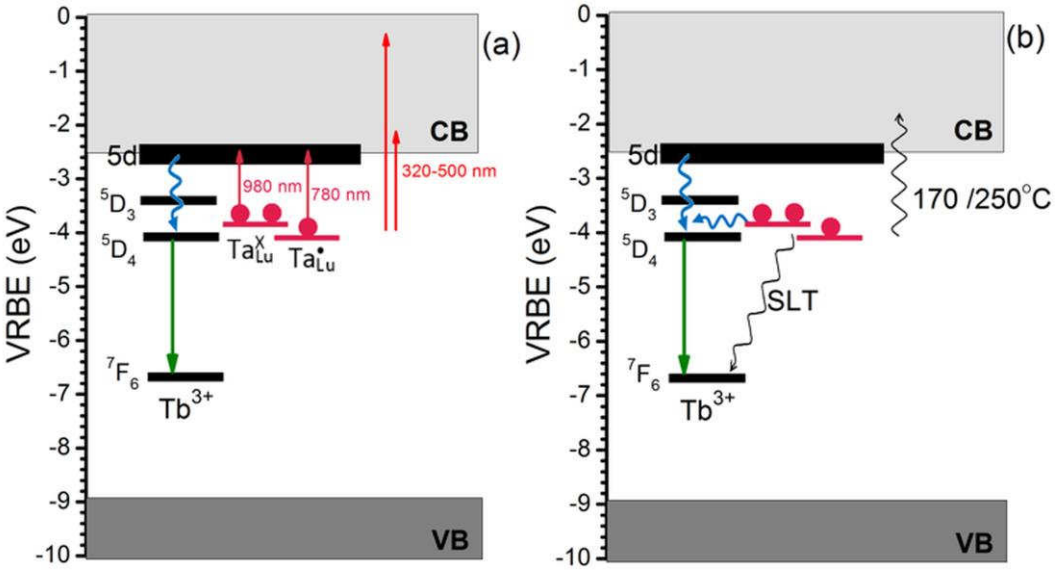

Fig. 11. *VRBE level schemes of Lu_2O_3:Tb,Ta storage phosphor. (a) shows the main processes during various optical stimulations and (b) presents in a simplified way the regular first-order kinetics TL process and the competing SLT mechanism. See text for details.*

The new data presented in this paper accord with the previously proposed carriers trapping model as mentioned in Introduction [24]. It is noteworthy, that after electron trapping tantalum reaches a state analogous to what would occur during $O^{2-}\rightarrow$Ta(V) charge transfer (CT) transition. An important difference is that in a regular CT excitation the system relaxes quickly to its ground state – the excited electron fills the hole. In the Lu_2O_3:Tb,Ta storage phosphor the quasi CT states, either $Ta^{\bullet}_{Lu}$or $Ta^{\times}_{Lu}$, retains kinetically stable because simultaneously hole is moved away to a Tb^{3+} ion converting it to $Tb^{\bullet}_{Lu}$ ($\equiv Tb^{4+}$). Thus, simultaneous trapping of electrons and holes *separates spatially* both carriers precluding their annihilation. However, when the trapping sites get sufficiently close each other the trapped carriers may interact and annihilate without an external stimulation. This explains why with increasing concentration of the dopants the capability of carriers trapping quickly diminishes to become totally inefficient when their contents reach 1 %.

Let us finally note that all findings and conclusions presented above agree very well with the model developed within the last decade by Dorenbos [17][55–58]. It predicts that $Tb^{\times}_{Lu}$ in Lu_2O_3

is a potential deep hole trap with a depth of ~2.2 eV, much deeper than electron traps related to Ta found in our experiments. After trapping a hole the positive net charge of $Tb^{\bullet}_{Lu}$ makes this center attractive to negatively charged electrons released, thermally or optically, from their traps. This only facilitates their mutual interaction to generate Tb^{3+}*. The same model foresees that Ta(V) impurity should generate electron traps in oxide hosts [59] introducing empty levels below hosts conduction band, exactly as is seen in Lu_2O_3:Tb,Ta. Upon the data presented in [59] the depth of $Ta^{\bullet}_{Lu}$ can be estimated at ~0.8 eV, which is 0.38 eV less than the value found experimentally in this research (1.18 eV). Since both numbers are burdened with some inaccuracy it may be accepted that the semi empirical model presented by Dorenbos and our experimental data agrees well and support each other.

Also the anomalous heating rate dependence (Fig. 6) can be justified taking into account the spatially spread character of $Ta^{\bullet}_{Lu}$ and $Ta^{\times}_{Lu}$ states generated after carriers trapping. Upon slow heating there is more time for interaction between trapped holes and electrons and their annihilation, presumably nonradiative, before the latter gets to conduction band. Faster heating favors the opposite situation - exactly as SLT model predict. At RT the 0.5 % ceramics showed radiative fading by means of tunneling (Fig. 7c). This is justified by the similarity of the energetic position of the Ta-related traps with the $^5D_4$ level of Tb^{3+}, see Fig. 11. All what is needed is a spatial correlation of the two traps, which is more probably as the concentration of both dopants increases. Then, by tunneling, the electron density may be transferred from the electron trap to the emitting level of Tb^{3+} according to Eq. 2:

$$Tb^{\bullet}_{Lu} + Ta^{\bullet}_{Lu} \rightarrow Tb^{\times}_{Lu}{}^{*} + Ta^{\bullet\bullet}_{Lu}. \qquad (2)$$

Finally, the $Tb^{\times}_{Lu}$* relaxes emitting a photon of light. The energetic proximity of Tb^{3+} $^5D_4$ level and $Ta^{\times}_{Lu}$ (two electrons trapped) allows for analogous tunneling between these two entities.

We yet wish to comment on the role of Ta(V) in the system. The $Ta_{Lu}^{\bullet\bullet}$ (before electron(s) trapping), due to its high positive local charge and the size smaller by about 21 % [60] than the substituted Lu^{3+}, necessarily drains the density of electron cloud from the adjacent O^{2-} ions. Consequently, the positive net charge of $Ta_{Lu}^{\bullet\bullet}$ is spread over the oxygen ligands too. Then, when the electron from the conduction band gets trapped its charge density may be distributed over the $Ta_{Lu}^{\bullet\bullet}$ and its nearest neighborhood – oxygen ligands. Calculations for HfO_2 showed that even holes, much heavier and more localized than electrons, may be trapped sharing density with a few adjacent oxygen atoms [61]. It does not change the fact that this is the $Ta_{Lu}^{\bullet\bullet}$ which predominantly shapes the electron trapping center properties.

5. Conclusions

Detailed analysis of thermoluminescent properties of Lu_2O_3:Tb,Ta ceramics were performed using optical and thermoluminescent techniques. The first order Randall-Wilkins mechanism of TL was proved to be accompanied with semi-localized transitions. The latter was blamed responsible for very significant fading of TL signal above 0.1 % of activator concentrations. However, the room temperature fading in the 0.5 % ceramics occurred partially by radiative tunneling. In contrary to TL, photoluminescence of Tb^{3+} was found to be quite resistant to concentration quenching up to 1 % of Tb and Ta contents. All that prove that efficiency of carriers trapping lessens when the trapping sites are not considerably distanced. Optically stimulated luminescence confirmed that the main traps giving TL peaks around 170 °C and 250 °C (for β=5 °C/s) have depths about 1.2 eV and 1.4 eV. Good agreement was found between the experimental data reported here and predictions from the semi empirical model of Dorenbos.

Acknowledgments

The authors gratefully acknowledge financial support by the Polish National Science Centre (NCN) under the grant #UMO-2014/13/B/ST5/01535. Synchrotron experiments were

performed at DESY-HasyLab laboratory in Hamburg under the project #II-20090289 EC supported by European Union.

References

[1] M. Guzik, G. Alombert-Goget, Y. Guyot, J. Pejchal, A. Yoshikawa, A. Ito, T. Goto, G. Boulon, Spectroscopy of C_{3i} and C_2 sites of Nd^{3+}-doped Lu_2O_3 sesquioxide either as ceramics or crystal, J. Lumin. 169 (2016) 606–611.

[2] S. Kurosawa, L. An, A. Yamaji, A. Suzuki, Y. Yokota, K. Shirasaki, T. Yamamura, A. Ito, T. Goto, G. Boulon, A. Yoshikawa, Scintillation Properties of Nd^{3+} -Doped Lu_2O_3 Ceramics in the Visible and Infrared Regions, IEEE Trans. Nucl. Sci. 61 (2014) 316–319.

[3] A. Wiatrowska, E. Zych, Traps Formation and Characterization on Long-Term Energy Storing Lu_2O_3:Pr,Hf Luminescent Ceramics, J. Phys. Chem. C. 117 (2013) 26921–26928.

[4] D. Kulesza, P. Bolek, A.J.J. Bos, E. Zych, Lu_2O_3-based storage phosphors. An (in)harmonious family, Coord. Chem. Rev. 325 (2016) 29–40.

[5] C.C.S. Pedroso, J.M. Carvalho, L.C.V. Rodrigues, J. Hölsä, H.F. Brito, Rapid and Energy-Saving Microwave-Assisted Solid-State Synthesis of Pr^{3+} -, Eu^{3+} -, or Tb^{3+} -Doped Lu_2O_3 Persistent Luminescence Materials, ACS Appl. Mater. Interfaces. 8 (2016) 19593–19604.

[6] V. V. Nagarkar, S.R. Miller, S. V. Tipnis, A. Lempicki, C. Brecher, H. Lingertat, A new large area scintillator screen for X-ray imaging, Nucl. Instruments Methods Phys. Res. Sect. B. 213 (2004) 250–254.

[7] A. Lempicki, C. Brecher, P. Szupryczynski, H. Lingertat, V. V. Nagarkar, S. V. Tipnis, S.R. Miller, A new lutetia-based ceramic scintillator for X-ray imaging, Nucl. Instruments Methods Phys. Res. Sect. A. 488 (2002) 579–590.

[8] C. Brecher, R.H. Bartram, A. Lempicki, Hole traps in Lu_2O_3:Eu ceramic scintillators. I.

Persistent afterglow, J. Lumin. 106 (2004) 159–168.

[9] V. V. Nagarkar, S. V. Tipnis, S.R. Miller, A. Lempicki, C. Brecher, P. Szupryczynski, H. Lingertat, A New X-Ray Scintillator for Digital Radiography, IEEE Trans. Nucl. Sci. 50 (2003) 297–300.

[10] E. Zych, J. Trojan-Piegza, L. Kępiński, Homogeneously precipitated Lu_2O_3:Eu nanocrystalline phosphor for X-ray detection, Sensors Actuators B. 109 (2005) 112–118.

[11] J. Trojan-Piegza, E. Zych, J. Hölsä, J. Niittykoski, Spectroscopic Properties of Persistent Luminescence Phosphors: $Lu_2O_3:Tb^{3+},M^{2+}$ (M=Ca,Sr,Ba), J. Phys. Chem. C. 113 (2009) 20493–20498.

[12] J. Trojan-Piegza, J. Niittykoski, J. Hölsä, E. Zych, Thermoluminescence and Kinetics of Persistent Luminescence of Vacuum-Sintered Tb^{3+} -Doped and Tb^{3+},Ca^{2+} -Codoped Lu_2O_3 Materials, Chem. Mater. 20 (2008) 2252–2261.

[13] D. Kulesza, E. Zych, Managing the properties of Lu_2O_3:Tb,Hf storage phosphor by means of fabrication conditions, J. Phys. Chem. C. 117 (2013) 26921–26928.

[14] E. Zych, J. Trojan-Piegza, D. Hreniak, W. Strek, Properties of Tb-doped vacuum-sintered Lu_2O_3 storage phosphor, J. Appl. Phys. 94 (2003) 1318–1324.

[15] E. Zych, D. Kulesza, Energy recovery from Lu_2O_3:Tb,Hf ceramic storage phosphors, Zeitschrift Fur Naturforsch. - Sect. B J. Chem. Sci. 69 (2014) 165–170.

[16] D. Kulesza, J. Trojan-Piegza, E. Zych, Lu_2O_3:Tb,Hf storage phosphor, Radiat. Meas. 45 (2010) 490–492.

[17] P. Dorenbos, A.J.J. Bos, Lanthanide level location and related thermoluminescence phenomena, Radiat. Meas. 43 (2008) 139–145.

[18] A.J.J. Bos, P. Dorenbos, A. Bessire, A. Lecointre, M. Bedu, M. Bettinelli, F. Piccinelli, Study of TL glow curves of YPO_4 double doped with lanthanide ions, Radiat. Meas. 46 (2011) 1410–1416.

[19] H. Luo, A.J.J. Bos, P. Dorenbos, Charge Carrier Trapping Processes in RE_2O_2S (RE=La, Gd, Y and Lu), J. Phys. Chem. C. 121 (2017) 8760–8769.

[20] P. Dorenbos, Charge transfer bands in optical materials and related defect level location, Opt. Mater. (Amst). 69 (2017) 8–22.

[21] P. Dorenbos, A Review on How Lanthanide Impurity Levels Change with Chemistry and Structure of Inorganic Compounds, ECS J. Solid State Sci. Technol. 2 (2013) R3001–R3011.

[22] T. Lyu, P. Dorenbos, Charge carrier trapping processes in lanthanide doped $LaPO_4$, $GdPO_4$, YPO_4, and $LuPO_4$, J. Mater. Chem. C. 6 (2018) 369–379.

[23] H. Luo, A.J.J. Bos, P. Dorenbos, Controlled Electron-Hole Trapping and Detrapping Process in $GdAlO_3$ by Valence Band Engineering, J. Phys. Chem. C. 120 (2016) 5916–5925.

[24] E. Zych, P. Bolek, D. Kulesza, On thermoluminescence of Lu_2O_3:Tb,Ta ceramic storage phosphors, J. Lumin. 189 (2017) 153–158.

[25] M.L. Mah, P.R. Armstrong, S.S. Kim, J.R. Carney, J.M. Lightstone, J.J. Talghader, Sensing the Thermal History of High-Explosive Detonations Using Thermoluminescent Microparticles, 13 (2013) 1742–1747.

[26] J.J. Talghader, M.L. Mah, E.G. Yukihara, A.C. Coleman, Thermoluminescent microparticle thermal history sensors, Microsystems Nanoeng. 2 (2016) 1–13.

[27] M.L. Mah, M.E. Manfred, S.S. Kim, M. Prokic, E.G. Yukihara, J.J. Talghader,

Measurement of Rapid Temperature Profiles Using Thermoluminescent Microparticles, IEEE Sens. J. 10 (2010) 311–315.

[28] M.L. Mah, P.R. Armstrong, S.S. Kim, J.R. Carney, J.M. Lightstone, J.J. Talghader, Thermal History Sensing inside High-Explosive Environments using Thermoluminescent Microparticles, IEEE Sensors. 70 (2011) 1269–1272.

[29] M.P. Pechini, Method of preparing lead and alkaline earth titanates and niobates and coating method using the same to form a capacitor, U.S. Pat. N^{o} 3,330.697. (1967).

[30] G. Zimmerer, Status report on luminescence investigations with synchrotron radiation at HASYLAB, Nucl. Inst. Methods Phys. Res. A. 308 (1991) 178–186.

[31] J. Zeler, L.B. Jerzykiewicz, E. Zych, Flux-Aided Synthesis of Lu_2O_3 and Lu_2O_3:Eu—Single Crystal Structure, Morphology Control and Radioluminescence Efficiency, Materials (Basel). 7 (2014) 7059–7072.

[32] M. Guzik, J. Pejchal, A. Yoshikawa, A. Ito, T. Goto, M. Siczek, T. Lis, G. Boulon, Structural Investigations of Lu_2O_3 as Single Crystal and Polycrystalline Transparent Ceramic, Cryst. Growth Des. 14 (2014) 3327–3334.

[33] G. Concas, G. Spano, E. Zych, J. Trojan-Piegza, Nano- and microcrystalline Lu_2O_3 :Eu phosphors: variations in occupancy of C_2 and S_6 sites by Eu^{3+} ions, J. Phys. Condens. Matter. 17 (2005) 2597–2604.

[34] E. Zych, J. Trojan-Piegza, Anomalous activity of Eu^{3+} in S_6 site of Lu_2O_3 in persistent luminescence, J. Lumin. 122–123 (2007) 335–338.

[35] J. Trojan-Piegza, E. Zych, Afterglow luminescence of Lu_2O_3:Eu ceramics synthesized at different atmospheres, J. Phys. Chem. C. 114 (2010) 4215–4220.

[36] E. Zych, J. Trojan-Piegza, Low-Temperature Luminescence of Lu_2O_3:Eu Ceramics

upon Excitation with Synchrotron Radiation in the Vicinity of Band Gap Energy, Chem. Mater. 18 (2006) 2194–2199.

[37] P. Dorenbos, Modeling the chemical shift of lanthanide 4f electron binding energies, Phys. Rev. B - Condens. Matter Mater. Phys. 85 (2012) 1–10.

[38] G. Blasse, B.C. Grabmaier, Luminescent Materials, Springer-Verlag, Berlin Heidelberg, 1994.

[39] R.T. Wegh, A. Meijerink, Spin-allowed and spin-forbidden $4f^n$-$4f^{n-1}5d$ transitions for heavy lanthanides in fluoride hosts, Phys. Rev. B. 60 (1999) 10820–10830.

[40] L. Van Pieterson, M.F. Reid, G.W. Burdick, A. Meijerink, $4f^n$-$4f^{n-1}5d$ transitions of the heavy lanthanides: Experiment and theory, Phys. Rev. B - Condens. Matter Mater. Phys. 65 (2002) 1–13.

[41] J.T. Randall, M.H.F. Wilkins, Phosphorescence and Electron Traps. I. The Study of Trap Distributions, Proc. R. Soc. A Math. Phys. Eng. Sci. 184 (1945) 365–389.

[42] S.W.S. McKeever, Thermoluminescence of Solids, Cambridge University Press, Cambridge, U.K, 1985.

[43] A. Halperin, A.A. Braner, Evaluation of Thermal Activation Energies from Glow Curves, Phys. Rev. 117 (1960) 408–415.

[44] E. Zych, A. Meijerink, C.D.M. Donega, Quantum efficiency of europium emission from nanocrystalline powders of Lu_2O_3:Eu, J. Phys. Condens. Matter. 15 (2003) 5145–5155.

[45] R. Chen, S.W.S. McKeever, Theory of thermoluminescence and related phenomena, World Scientific Publishing, 1997.

[46] A.J.J. Bos, Theory of thermoluminescence, Radiat. Meas. 41 (2007) 45–56.

[47] R. Chen, V. Pagonis, Thermally and Optically Stimulated Luminescence: A Simulation Approach, John Wiley & Sons Ltd, USA, 2011.

[48] A. Mandowski, Semi-localized transitions model for thermoluminescence, J. Phys. D. Appl. Phys. 38 (2005) 17–21.

[49] A. Mandowski, Semi-localized transitions model-General formulation and classical limits, Radiat. Meas. 43 (2008) 199–202.

[50] A. Mandowski, A.J.J. Bos, Explanation of anomalous heating rate dependence of thermoluminescence in $YPO_4:Ce^{3+},Sm^{3+}$ based on the semi-localized transition (SLT) model, Radiat. Meas. 46 (2011) 1376–1379.

[51] V. Pagonis, L. Blohm, M. Brengle, G. Mayonado, P. Woglam, Anomalous heating rate effect in thermoluminescence intensity using a simplified semi-localized transition (SLT) model, Radiat. Meas. 51–52 (2013) 40–47.

[52] P. Bolek, D. Kulesza, A.J.J. Bos, E. Zych, The role of Ti in charge carriers trapping in the red-emitting Lu_2O_3:Pr,Ti phosphor, J. Lumin. 194 (2018) 641–648.

[53] J. Zeler, E. Zych, On the thermoluminescence properties and mechanism of $LuPO_4$:Eu sintered materials, RSC Adv. 6 (2016) 89019–89027.

[54] K. Van Den Eeckhout, A.J.J. Bos, D. Poelman, P.F. Smet, Revealing trap depth distributions in persistent phosphors, Phys. Rev. B - Condens. Matter Mater. Phys. 87 (2013) 1–11.

[55] A.H. Krumpel, E. van der Kolk, E. Cavalli, P. Boutinaud, M. Bettinelli, P. Dorenbos, Lanthanide 4f-level location in $AVO_{(4)}:Ln^{(3+)}$ (A=La, Gd, Lu) crystals, J. Phys. Condens. Matter. 21 (2009) 115503.

[56] A.J.J. Bos, P. Dorenbos, A. Bessière, B. Viana, Lanthanide energy levels in YPO_4, Radiat. Meas. 43 (2008) 222–226.

[57] P. Dorenbos, T. Shalapska, G. Stryganyuk, A. Gektin, A. Voloshinovskii, Spectroscopy and energy level location of the trivalent lanthanides in $LiYP_4O_{12}$, J. Lumin. 131 (2011) 633–639.

[58] T. Shalapska, P. Dorenbos, A. Gektin, G. Stryganyuk, A. Voloshinovskii, Luminescence spectroscopy and energy level location of lanthanide ions doped in $La(PO_3)_3$, J. Lumin. 155 (2014) 95–100.

[59] E.G. Rogers, P. Dorenbos, Vacuum Referred Binding Energy of the Single 3d, 4d, or 5d Electron in Transition Metal and Lanthanide Impurities in Compounds, ECS J. Solid State Sci. Technol. 3 (2014) R173–R184.

[60] R.D. Shannon, Revised effective ionic radii and systematic studies of interatomic distances in halides and chalcogenides, Acta Crystallogr. Sect. A. 32 (1976) 751–767.

[61] K. Fiaczyk, A.J. Wojtowicz, W. Drozdowski, K. Brylew, E. Zych, Thermoluminescent properties of HfO_2:Ti after exposure to X-rays, Radiat. Meas. 90 (2016) 140–144.